HHS Public Access

Author manuscript

Ann Biomed Eng. Author manuscript; available in PMC 2017 March 01.

Published in final edited form as:

Ann Biomed Eng. 2016 March ; 44(3): 621–635. doi:10.1007/s10439-015-1495-0.

Non-invasive and non-destructive characterization of tissue engineered constructs using ultrasound imaging technologies: a review

Kang Kim[a,b,d,1] and **William R. Wagner**[b,c,d]

[a]Center for Ultrasound Molecular Imaging and Therapeutics, Department of Medicine, University of Pittsburgh School of Medicine; Heart and Vascular Institute, University of Pittsburgh Medical Center (UPMC), Pittsburgh, PA 15213, USA

[b]Department of Bioengineering, University of Pittsburgh School of Engineering, Pittsburgh, PA 15213, USA

[c]Department of Surgery, University of Pittsburgh School of Medicine, Pittsburgh, PA 15213, USA

[d]McGowan Institute for Regenerative Medicine, University of Pittsburgh and UPMC, Pittsburgh, PA 15219, USA

Abstract

With the rapid expansion of biomaterial development and coupled efforts to translate such advances toward the clinic, non-invasive and non-destructive imaging tools to evaluate implants in situ in a timely manner are critically needed. The required multilevel information is comprehensive, including structural, mechanical, and biological changes such as scaffold degradation, mechanical strength, cell infiltration, extracellular matrix formation and vascularization to name a few. With its inherent advantages of non-invasiveness and non-destructiveness, ultrasound imaging can be an ideal tool for both preclinical and clinical uses. In this review, currently available ultrasound imaging technologies that have been applied in vitro and in vivo for tissue engineering and regenerative medicine are discussed and some new emerging ultrasound technologies and multi-modality approaches utilizing ultrasound are introduced.

Keywords

ultrasound imaging; noninvasive; nondestructive; multi-modality; tissue scaffolds; regeneration

1. Introduction

In tissue engineering, scaffolds are designed from biodegradable materials to support tissue growth, extracellular matrix (ECM) elaboration, and the eventual maturation or conversion of the implanted construct toward functional, native tissue. The remodeling process is

[1]Corresponding author. Center for Ultrasound Molecular Imaging and Therapeutics, University of Pittsburgh and UPMC, Pittsburgh, PA 15213, USA. Tel.: +1 412 624 5092; fax: +1 412 624 2264. kangkim@upmc.edu. .

dynamic and complex, dependent not only on the scaffold chemistry and morphology, but on the host implant site, inflammatory response, mechanical environment, and disease state, to name but a few important parameters. Despite this complex situation, scaffold design principles provide some general options in terms of chemistry and processing to tune degradation, provided sufficient in vivo data are available to guide such design modifications. The collection of such in vivo data often requires destructive analysis and substantial animal use to allow the construct to be explanted and characterized histologically and mechanically. [43, 88, 79, 37] Ideally, non-invasive methods would allow monitoring of the scaffold site in situ and temporally, allowing longitudinal studies and consequently reducing animal use and shortening study time.

Several different groups of biomaterials, primarily ceramics, and polymers of synthetic or natural origin (e.g. collagen) have been used in the fabrication of porous scaffolds for tissue engineering. There also has been growing interest in the use of a variety of animal-based decellularized tissues, in vitro-cultured cell sheets together with their secreted extracellular matrix (ECM), or this in vitro-derived ECM alone after cell removal.[13] As proteins such as growth factors, adhesion peptides, and cytokines play a central role in the natural tissue regeneration and repair process, [76] delivering such bioactive agents in the context of the aforementioned scaffolds has also received considerable attention. [59],[26]

With such a rapidly diversifying set of approaches in regenerative medicine to scaffold materials, delivery approaches, and targeted tissues, a common theme remains the assessment of the implanted construct transition toward (hopefully) a functional scaffold that is mechanically appropriate and integrated with the surrounding tissue. This remains true as tissue engineering approaches are beginning to translate towards some promising clinical applications.[25],[11],[54],[83] It is in this current state of the field where a need remains for a non-invasive, non-destructive, and non-ionizing imaging tool that could provide design feedback, treatment monitoring, and intervention guidance, particularly from a mechanical perspective, in both pre-clinical and clinical models.

Biomedical ultrasound imaging is based on the measurement of ultrasound waves as they interact with tissues. Among several common non-invasive imaging modalities, ultrasound imaging stands out as an ideal candidate for tissue engineering and regenerative medicine. Not only does ultrasound imaging provide the inherent advantages associated with non-invasiveness and non-destructiveness, but at low cost it provides real-time temporal resolution and relatively high spatial resolution with advances in transducer arrays and related beamforming technologies. As such, ultrasound has been widely used in clinics for decades. Ultrasound imaging now has a well-established place in clinical practice such that it currently accounts for about one in four of all imaging procedures worldwide[82], thus it is expected to be highly translatable for tissue engineering and regenerative medicine applications.

Current imaging strategies for tissue engineering and regenerative medicine have recently been summarized by Nam et al.[52] and Appel et al.[3] in their review papers where different imaging modalities for various applications in tissue engineering and regenerative medicine were discussed along with their strengths and weaknesses. Successful applications for

different levels of information including construct morphological and functional changes, tissue formation through growth factor release and cell infiltration, and the therapeutic outcomes were introduced. These applications in vitro and in vivo cover a wide range from subcellular to whole body in animal model as well as some human subject study. In addition, the potential of some emerging new technologies were introduced.

The objective in this review will be to focus on ultrasound imaging technologies that have been applied for tissue engineering and regenerative medicine purposes and introduce new emerging ultrasound-based technologies and their potential applications in this growing field. In addition to conventional B-scan and Doppler imaging for structural and physiological information, respectively, ultrasound elasticity imaging that includes compressional elasticity imaging and shear wave elasticity imaging for mechanical property assessment, tissue characterization for cell density and ECM elaboration, and novel photoacoustic imaging (PAI) for vascularization, cell tracking, and scaffold degradation will be discussed. These imaging modalities have high potential for ultimate use in both pre-clinical and clinical studies in the area of tissue engineering and regenerative medicine.

2. Back scattering imaging

Backscattered ultrasound from soft tissues allows for the formation of anatomical images based on conventional gray-scale brightness, while advanced signal processing techniques facilitate a more thorough analysis of characteristics such as cell density and ECM elaboration and other morphological features. For instance, the spectral parameters of backscattered ultrasound such as slope and mid-band fit (MBF) are known to be related to tissue microstructural properties such as size, concentration, and acoustic impedance.[39,39] These parameters have been used for assessing tissue characteristics, including cancers[22,18] and intravascular plaques.[49,53] Similar imaging techniques that utilize the spectral analysis of raw ultrasound backscattered radio frequency (RF) data can characterize microstructural properties of engineered tissue constructs. While gray-scale analysis is relatively straightforward using commercially available ultrasound scanners, the results can be either operator or system dependent. Spectral analysis that can be calibrated to the ultrasound system provides more instrument-independent measurements, while it requires an ultrasound system that provides an RF signal access and more intensive post signal processing.

Continued monitoring of such parameters can provide important information about how implanted scaffolds are interacting with surrounding native tissues and about the pace and extent of the regeneration processes. In vitro, in order to achieve high spatial resolution, a very high frequency (> 50 MHz) single element ultrasound transducer is generally used, while preclinical or clinical imaging is performed using either a commercial transcutaneous array transducer in mid-range frequency (2-10 MHz) for a larger imaging depth or a catheter-based intravascular ultrasound system (IVUS) with a high frequency (15-30 MHz or above).

The collagen content in tissue-engineered constructs based on fibrin [34] and ECM deposition [19,73] have been quantitatively analyzed with gray-scale ultrasound scans in which the change of ultrasound signal intensity reflects the gradual increase in density of cells or

extracellular proteins. Using an ultrasound microscopy system with a high frequency (50 MHz) single element transducer, Winterroth et al. imaged the surface irregularities of an ex vivo produced oral mucosal equivalent developed on a cellular cadaveric dermis, as seeded cells adhered and grew and a keratinized protective outermost layer formed.[85] In other in vitro work, by estimating the sound speed and the attenuation in each section of the explanted constructs using high-frequency ultrasound microscopy, the distribution of nonhomogeneous tissue content in tissue-engineered scaffolds made from various polymers loaded with chondrocytes/atelocollagen mixture were examined two months after implantation in the subcutaneous space of nude mice.[75] High-frequency ultrasound backscatter measurements over a broad range of frequencies (13- 47 MHz) were able to quantify the cell concentration from cell-embedded, 3-D agarose hydrogels in vitro. [48](Fig. 1A) Similarly, high resolution spectral ultrasound imaging (SUSI) was used to monitor the differentiation of MC3T3 pre-osteoblasts seeded within collagen hydrogels, providing the number and differentiation state of the cells[23](Fig.1B) and mineralization in collagen hydrogels.[18] Comparing measurements at 50 MHz and 100 MHz when analyzing the sound speed and the attenuation slope in the gels allowed for in vitro assessment of the degradation of chondrocyte encapsulated hydrogel.[67]

Ultrasound gray-scale imaging has also been used for longitudinal assessment of adipose tissue engineering[78] and tissue engineering techniques applied to ischemic cardiomyopathy[29] in preclinical animal studies. Ultrasound imaging, specifically serial intravascular ultrasound imaging (IVUS), has been employed to evaluate the evolution of atherosclerotic plaque in coronary bifurcations after implanting a bioresorbable scaffold in human subjects. IVUS-virtual histology (VH) allowed identification of four plaque components: dense calcium, necrotic core, fibrofatty and fibrotic tissue that are illustrated in a color coded map.[36] (Fig.2)

3. Doppler imaging

The capability to measure hemodynamic information, such as blood perfusion of the micro-vasculature growing into an implant site, the patency and blood flow in tissue engineered vascular grafts and the flow patterns associated with tissue engineered heart valves, is critically needed to evaluate tissue construct success over time. Doppler ultrasound imaging, which is one of the standard imaging modes in most commercial ultrasound scanners, allows for visualization of local fluid flow in a non-invasive manner. Of course, patency of vascular grafts can still be examined by using gray-scale brightness to identify the open lumen area of the vessels, but sensitivity is greatly limited. [27,44,65] For instance, blood flow in acellular vascular grafts engineered with collagen-elastin composites that was implanted in the rat infrarenal aortic position, was monitored using Doppler ultrasound imaging by Kumar et al.[35] Several other studies have similarly used Doppler ultrasound imaging in pre-clinical studies to evaluate patency and flow in tissue-engineered vascular grafts, both in vitro and in vivo. [4, 77,86,2] Ultrasound Doppler imaging has also been utilized to effectively monitor the mechanical stability of tissue-engineered vascular grafts that was implanted to serve as arteriovenous shunts in end-stage renal disease patients[47] and also in this application area to monitor blood flow and to detect potential aneurysms or wall degradation in allogeneic tissue-engineered vascular grafts.[87] (Fig.3A)

Microvasculature can be visualized with significantly enhanced sensitivity of Doppler imaging through the use of exogenous imaging contrast agents, mostly microbubbles. Microbubbles have been injected into extracellular matrix scaffolds to measure flow rates and image microvessel network in 3D, characterizing their volume and size, and delineating the background matrix from the vascular circuits.[21] (Fig.3B) Nonlinear harmonic imaging with microbubbles has been applied to assess vascularization of hydrogels in vivo as well.[28] In some commercial ultrasound scanners, nonlinear harmonic imaging mode for use of microbubbles is available. In addition, Doppler ultrasound imaging can be used to demonstrate the function of a tissue-engineered heart valve, as has been shown with a tubular leaflet design in a flow-loop bioreactor with the injection of air bubbles.[81]

4. Elasticity imaging

A degradable scaffold is implanted to serve a mechanical role while the new tissue assumes the physiological load as the scaffold degrades. If this mechanical hand off fails, the consequences are often dire, resulting in failure of the procedure. As such, the degradation rate of the scaffold is of paramount importance for the long-term performance of tissue-engineered constructs in vivo. Accurate in vivo temporal data for scaffold degradation and load-bearing tissue growth are required for the rational design of scaffolds used in mechanically loaded tissues. Ideally, tissue engineers would be able to monitor construct remodeling in the same specimen over time. Elasticity imaging techniques using ultrasound is a well-suited candidate for this purpose.

A. Compressional ultrasound elasticity imaging

Ultrasound elasticity imaging (UEI), also known as ultrasound elastography, or sono-elastography, has the potential to become a valuable tool for monitoring the mechanical and structural changes of implanted engineered tissues at reasonably high spatial resolution with substantial imaging depth. Since it was introduced in the early 1990s as a non-invasive tool to investigate the mechanical properties of biological tissues,[38, 61, 72] UEI has been applied in a wide spectrum of applications for native tissues and organs in vitro and in vivo.[20], [66], [24],[31] While many unique signal processing procedures have been adopted in each new applied approach, the most commonly used elasticity imaging techniques are based on 2-D correlation-based speckle tracking methods. [33, 60, 6,40] Over the past several years, UEI based on speckle tracking has been shown to have great potential for clinical use, but mostly in applications involving native tissues.[64, 45, 70,42]

For high spatial resolution, an ultrasound microscopy system with a high frequency (50 MHz) single element transducer was used to obtain strain images of a tissue-engineered smooth muscle sample which clearly identified a several hundred micron thick cell layer that exhibited a different stiffness from its supporting matrix.[1] Using the same system, Winterroth *et al.* later monitored changes in the morphology and nonlinear elastic properties of engineered oral mucosal tissues under normal and thermally stressed culture conditions.[84] In vivo,[30] UEI using a commercial array transducer was applied to detect the degradation of the poly(1,8-octanedio-co-citrate) polymer scaffolds subcutaneously implanted in the backs of mice. With limited sample numbers and time points, the results supported the feasibility of UEI as a non-invasive monitoring tool for mechanical property changes of tissue

scaffolds in vivo. The change in strains from UEI due to scaffold degradation compared well with direct mechanical measurements; however, any tissue in-growth was not included in the investigation. To systematically investigate the correlation of the dynamic, adaptive mechanical and structural property changes with varying rates of scaffold degradation and tissue in-growth, porous scaffolds made from three biodegradable elastomers with different degradation rates were used in a later study: poly(ether ester urethane) urea (PEEUU) for a fast degradation rate, poly(ester urethane) urea (PEUU) for a moderate degradation rate and poly(carbonate urethane) urea (PCUU) for a slow degradation rate.[89]

These three different types of scaffolds were implanted as full thickness replacements of the rat muscular abdominal wall, and then UEI was systematically applied with a high frequency ultrasound scanner at time points for up to 12 weeks. As shown in Fig. 4A below, changes in scaffold morphology and stiffness were observed as time passed with scaffolds becoming smaller and thinner as the degradation progressed. Mechanically, the tissue constructs became harder or softer with time as indicated by the average normalized strain in Fig. 4B (a), indicating overall stiffness changes of the tissue constructs, while the surrounding native tissue stiffness remained near constant. From compression testing in Fig. 4B (b) the temporal changes in overall compliance correlated well with strains measured from UEI in Fig. 4B (a). In Fig. 4 B (c), the normalized strain values from UEI and the compliance from the compression tests exhibited a strong linear relationship. This study demonstrates the ability of nondestructive ultrasound methodology to provide an alternative method for the assessment of mechanical behavior as three different types of elastic, biodegradable scaffolds remodeled in a mechanically loaded environment in situ.

Although UEI has great potential to benefit preclinical animal studies and eventually be translated into the clinic, the technique has some inherent limitations: 1) the application is limited to areas where physical compression can be easily applied, 2) the normalization of the measured strain developed inside the constructs to the overall applied strain to the animal body can produce error, and 3) the measured strain can be subjective to the boundary conditions associated with applied force and surrounding anatomy.[89, 30,3] It should however be noted that in cardiovascular applications where physiologic pulsatile pressure can be used as the tissue deformation source, external mechanical compression is not required.[15,2]

B. Ultrasound shear wave elasticity imaging

Ultrasound shear wave elasticity imaging (USWEI), also known as transient elasticity imaging or supersonic shear wave imaging can be an alternative to UEI because this technique employs a remote palpation and provides absolute elastic modulus that can be reconstructed from the shear wave propagation speed measurements, provided the density of the tissue is known. The shear wave propagation speed is directly related to shear modulus of the underlying tissue.[71] The shear modulus of the target tissue can be reconstructed from the displacement field of the propagating shear waves using the Helmholtz inversion equation[56,5] or time of flight estimation.[69]

In an in vivo study using the rat abdominal repair model [63], two biodegradable polymers with different mechanical property and degradation rates were implanted: the PEUU mentioned above, which is a relatively soft material and degrades at moderate rate and

polydioxanone (PDO), which is a stiff material but degrades rapidly. Fig. 5A provides representative shear modulus images overlaid on B-mode images of PEUU and PDO constructs over time that were implanted in the rat abdominal wall. The stiffness changed the most for both scaffold types in the first 8 weeks during which the PEUU stiffness first increased and then began to decrease at week 4, while PDO continued softening up to the eighth week. In Fig. 5B (a), the Young's modulus of the constructs measured by direct mechanical testing after explantation at weeks 0, 4, 8, and 12 is shown. In a control group of rats, the Young's modulus of the native abdominal wall remained unchanged over 20 weeks. In Fig. 5B (b), the average shear modulus obtained by USWEI of the constructs (red open triangle) and the adjacent, native tissue (blue open square) is plotted over time. Note the shear modulus in each construct shown in the white dashed circle and the native tissue area on the opposite side shown in the red dashed circle depicted in Fig. 5A was spatially averaged. The mean value was then taken over 10 samples. The stiffness for the PEUU scaffolds after 8-12 weeks was found to be similar to that of the native neighboring tissues. In contrast, for the faster degrading PDO scaffolds the stiffness continued to decrease and dropped below the surrounding native tissues after week 8. Scatter plots showing the relationship between the Young's modulus obtained by mechanical compression testing and the USWEI-derived shear modulus for the same samples and time points are shown in Fig. 5B (c).

A limitation in this method is that only the shear storage modulus was determined using an inversion of the Helmholtz equation and viscoelastic behavior and the shear loss modulus were not considered. Advanced shear wave analysis might be used to address the dispersive characteristics of the propagating shear wave in viscoelastic materials.[14] A more accurate estimate of shear modulus can be achieved using a more robust estimate of sheer wave speed, such as time of flight.[69] Shear modulus can be estimated with improved accuracy by applying spatially modulated ultrasound radiation force.[46]

Other novel, advanced ultrasound elasticity imaging technnologies and their derivatives can be applied in tissue engineering and regenerative medicine for their own advantages and applicability such as acoustic radiation force impulse imaging (ARFI) [57] and vibro-acoustograpy[17] among others. Ultrasound elastography is found in most commercial ultrasound scanners, and acoustic radiation force imaging and swear wave imaging have been implemented in a few commercial ultrasound scanners and the number continues to grow.

5. Multi-modality imaging approach

There are a variety of newly emerging approaches that aim to overcome the inherent limitations with individual imaging methods. Among them, one of the most promising technologies is photoacoustic imaging, which benefits from characteristics inherent to both acoustics and optics since the technology involves the conversion of optical to ultrasonic energy.[58,16,80,12,41] In this technique, photon energy delivered by a short laser pulse transiently increases the local temperature of target molecules in biological tissue that results in rapid thermal expansion.[16,80,12] The acoustic wave generated through this mechanical vibration can be detected by ultrasound sensors. Since ultrasound scattering in biological

tissue is less than optical scattering by three orders of magnitude, photoacoustic imaging depth can be much larger than optical microscopy. In addition, imaging depth and spatial resolution can be tradeoff with appropriate acoustic and optical design of the photoacoustic system. This allows for a wide range of photoacoustic imaging application from the subcellular scale to the whole animal level.[80] With aid of various endogenous contrast such as hemoglobin and melanin or exogenous contrast agents, including nanoparticles and dyes, photoacoustic imaging can provide functional and molecular/cellular information.[9,41,51] Imaging at various wavelengths opens further possibilities, such as the separate mapping of blood oxygen saturation and nanoparticle distribution.[32]

In tissue engineering applications, cell population inside engineered tissue constructs and its change over time have been successfully monitored by photoacoustic imaging in vitro with aid of exogenous photoacoustic contrast agents such as dyes or gold nanoparticles, or endogenous optical contrast by melanoma cells.[90,91,10] Gold nanoparticles have also been targeted to endothelial cells to enhance visualization of angiogenesis with photoacoustic microscopy(PAM) as demonstrated in vivo in a hydrogel scaffold containing FGF-2.[62] In vivo animal studies have been performed utilizing many different photoacoustic imaging systems at once that includes a photoacoustic microscopy (PAM) using a single element ultrasound transducer, B-mode cross sectional imaging a linear array ultrasound transducer, and tomography. PAM successfully visualized vasculature development and scaffold degradation in the nude mouse ear at high spatial resolution and sensitivity.[7,92] (Fig.6) When a ultrasound array transducer is used, with enhanced imaging depth, in vivo photoacoustic imaging can be applied in tissue regeneration studies in a rat model.[74,51] Mesenchymal stem cells that were labeled with gold nanoparticles and delivered to ischemic muscle in a PEGylated fibrin gel were successfully monitored in vivo.[50,68](Fig.7) Polymer scaffolds incorporated with single-walled carbon nanotubes, which enhance the photoacoustic signal as well as reinforce the mechanical properties of the scaffolds were imaged and compared with micro-CT for better imaging contrast and structural information.[7] In work related to that discussed for USWEI above, two types of biodegradable polymers with different stiffness and degradation rates stained with indocyanine green for optical contrast were monitored in vivo for their structural changes by photoacoustic imaging.[63](Fig. 8)

In other efforts to combine imaging modalities, changes in ECM content occurring during chondrogenic differentiation of equine adipose stem cells on 3D biodegradable matrices have been evaluated using a prototype system combining time-resolved fluorescence spectroscopy, fluorescence lifetime imaging microscopy, and ultrasound backscatter microscopy by Fite et al.[19] Using the same system, self-assembled engineered articular cartilage constructs treated with chemical agents for biochemical and subsequent mechanical changes were monitored in vitro by Sun et al. from the same group.[73] Non-invasive, non-destructive monitoring that couples structural degradation and mechanical strength changes in engineered tissue constructs would provide a pivotal tool for tissue engineers to evaluate and better design candidate scaffolds. Concurrent in vivo monitoring of both mechanical stiffness and structural changes were reported using photoacoustic imaging and shear wave elasticity imaging.[63] Integration of these two imaging technologies into a single ultrasound platform for automated co-registration has been introduced by Nguyen et al.[55] (Fig. 9)

Neovascularization of porous polymer foams implanted in mice ears has been monitored over a six-week time period using PAM and optical coherence tomography (OCT), with capillary-level resolution.[8] (Fig. 10)

6. Conclusion

Considering the rapidly increasing number of scaffold design and implantation approaches being proposed for regenerative medicine applications, there is a need for more effective non-invasive, non-destructive evaluation tools to maximize the quality of data coming from pre-clinical evaluations. Looking forward to the clinical setting, such non-invasive imaging tools will become critically necessary. Among currently available imaging modalities, weighing their advantages and disadvantages, ultrasound is an attractive choice for both pre-clinical and clinical uses in that it is non-invasive, nondestructive, affordable, and capable of real-time imaging. In this review some successful applications of ultrasound imaging techniques for monitoring engineered tissue constructs have been introduced. Depending on the required information for specific applications, selection of imaging techniques, sensors, systems, and associated parameters such as operating frequency should be carefully considered. In general, for in vitro examinations requiring high spatial resolution, ultrasound microscopic approaches with a high frequency transducer are attractive, while for in vivo study, mid or low frequency array transducers will provide enough depth information in exchange for a somewhat compromised spatial resolution. Except for the peripheral vascular grafts, intravascular ultrasound (IVUS) provides the needed accessibility to the deep major vessels with some compromise in invasiveness. In addition to morphological information, some currently available advanced ultrasound imaging technologies allow for measurement of important information such as cell density, vascularization and perfusion, and mechanical parameters for constructs in situ. Some of those imaging technologies have already been used on human subjects, providing a high likelihood of smooth translation of these technologies into clinics if needed. Ultrasound does have inherent limitations, providing only 2D cross-sectional imaging using a 1D array transducer, which can be responsible for the reported variability in study and clinical diagnosis. With the recent development of 2D array transducers, which are now commercially available, 3D volume imaging in real-time (4D) has been realized, albeit with a relatively low spatial resolution and limited contrast. To overcome these drawbacks and limitations, a multi-modal approach bringing to bear other imaging tools and techniques in concert with ultrasound is most promising. A few such novel approaches in combination with photoacoustics imaging, swear wave elasticity imaging, fluorescence imaging, and optical coherence tomography have shown promise in regenerative medicine applications. Further advances in ultrasound-based imaging are expected to appear in the coming years as investigators are constantly looking for methods that will provide better information on how implanted tissue constructs may or may not be remodeling in vivo to provide functionally beneficial and safe clinical outcomes.

Acknowledgements

This work was supported by NIH R21EB013353.

8. References

1. Abraham Cohn N, Kim B-S, Erkamp RQ, Mooney DJ, Emelianov SY, Skovoroda AR, O'Donnell M. High-resolution elasticity imaging for tissue engineering. IEEE Trans. Ultrason. Ferroelectr. Freq. Control. 2000; 47:956–966. [PubMed: 18238630]
2. Allen RA, Wu W, Yao M, Dutta D, Duan X, Bachman TN, Champion HC, Stolz DB, Robertson AM, Kim K, Isenberg JS, Wang Y. Nerve regeneration and elastin formation within poly(glycerol sebacate)-based synthetic arterial grafts one-year post-implantation in a rat model. Biomaterials. 2014; 35:165–173. [PubMed: 24119457]
3. Appel AA, Anastasio MA, Larson JC, Brey EM. Imaging challenges in biomaterials and tissue engineering. Biomaterials. 2013; 34:6615–6630. [PubMed: 23768903]
4. Assmann A, Akhyari P, Delfs C, Flögel U, Jacoby C, Kamiya H, Lichtenberg A. Development of a Growing Rat Model for the In Vivo Assessment of Engineered Aortic Conduits. J. Surg. Res. 2012; 176:367–375. [PubMed: 22172135]
5. Bercoff J, Tanter M, Fink M. Supersonic shear imaging: a new technique for soft tissue elasticity mapping. IEEE Trans. Ultrason. Ferroelectr. Freq. Control. 2004; 51:396–409. [PubMed: 15139541]
6. Bilgen M, Insana MF. Deformation models and correlation analysis in elastography. J. Acoust. Soc. Am. 1996; 99:3212–3224. [PubMed: 8642127]
7. Cai X, Paratala BS, Hu S, Sitharaman B, Wang LV. Multiscale photoacoustic microscopy of single-walled carbon nanotube-incorporated tissue engineering scaffolds. Tissue Eng. Part C Methods. 2012; 18:310–317. [PubMed: 22082018]
8. Cai X, Zhang Y, Li L, Choi S-W, MacEwan MR, Yao J, Kim C, Xia Y, Wang LV. Investigation of neovascularization in three-dimensional porous scaffolds in vivo by a combination of multiscale photoacoustic microscopy and optical coherence tomography. Tissue Eng. Part C Methods. 2013; 19:196–204. [PubMed: 22838500]
9. Cai X, Zhang YS, Xia Y, Wang LV. Photoacoustic microscopy in tissue engineering. Mater. Today. 2013; 16:67–77.
10. Chung E, Nam SY, Ricles LM, Emelianov SY, Suggs LJ. Evaluation of gold nanotracers to track adipose-derived stem cells in a PEGylated fibrin gel for dermal tissue engineering applications. Int. J. Nanomedicine. 2013; 8:325–336. [PubMed: 23345978]
11. Cicciù M, Herford AS, Cicciù D, Scott A, Cicciù D, Tandon R, Maiorana C. Recombinant human bone morphogenetic protein-2 promote and stabilize hard and soft tissue healing for large mandibular new bone reconstruction defects. J. Craniofac. Surg. 2014; 25:860–862. [PubMed: 24820713]
12. Cox B, Laufer JG, Arridge SR, Beard PC. Quantitative spectroscopic photoacoustic imaging: a review. J. Biomed. Opt. 2012; 17:0612021–06120222.
13. Dahl SLM, Kypson AP, Lawson JH, Blum JL, Strader JT, Li Y, Manson RJ, Tente WE, DiBernardo L, Hensley MT, Carter R, Williams TP, Prichard HL, Dey MS, Begelman KG, Niklason LE. Readily Available Tissue-Engineered Vascular Grafts. Sci. Transl. Med. 2011; 3:68ra9–68ra9.
14. Deffieux T, Montaldo G, Tanter M, Fink M. Shear Wave Spectroscopy for In Vivo Quantification of Human Soft Tissues Visco-Elasticity. IEEE Trans. Med. Imaging. 2009; 28:313–322. [PubMed: 19244004]
15. Dutta D, Lee K-W, Allen RA, Wang Y, Brigham JC, Kim K. Non-invasive Assessment of Elastic Modulus of Arterial Constructs during Cell Culture Using Ultrasound Elasticity Imaging. Ultrasound Med. Biol. 2013; 39:2103–2115. [PubMed: 23932282]
16. Emelianov SY, Li P-C, O'Donnell M. Photoacoustics for molecular imaging and therapy. Phys. Today. 2009; 62:34–39. [PubMed: 20523758]
17. Fatemi M, Greenleaf JF. Vibro-acoustography: An imaging modality based on ultrasound-stimulated acoustic emission. Proc. Natl. Acad. Sci. 1999; 96:6603–6608. [PubMed: 10359758]
18. Feleppa EJ. Ultrasonic tissue-type imaging of the prostate: implications for biopsy and treatment guidance. Cancer Biomark. Sect. Dis. Markers. 2008; 4:201–212.

19. Fite BZ, Decaris M, Sun Y, Sun Y, Lam A, Ho CKL, Leach JK, Marcu L. Noninvasive Multimodal Evaluation of Bioengineered Cartilage Constructs Combining Time-Resolved Fluorescence and Ultrasound Imaging. Tissue Eng. Part C Methods. 2011; 17:495–504. [PubMed: 21303258]
20. Gao L, Parker KJ, Lerner RM, Levinson SF. Imaging of the elastic properties of tissue—A review. Ultrasound Med. Biol. 1996; 22:959–977. [PubMed: 9004420]
21. Gessner RC, Hanson AD, Feingold S, Cashion AT, Corcimaru A, Wu BT, Mullins CR, Aylward SR, Reid LM, Dayton PA. Functional ultrasound imaging for assessment of extracellular matrix scaffolds used for liver organoid formation. Biomaterials. 2013; 34:9341–9351. [PubMed: 24011714]
22. Golub RM, Parsons RE, Sigel B, Feleppa EJ, Justin J, Zaren HA, Rorke M, Sokil-Melgar J, Kimitsuki H. Differentiation of breast tumors by ultrasonic tissue characterization. J. Ultrasound Med. 1993; 12:601–608. [PubMed: 8246339]
23. Gudur MSR, Rao RR, Peterson AW, Caldwell DJ, Stegemann JP, Deng CX. Quantification of In Vitro Osteoblastic Differentiation in 3D Engineered Tissue Constructs Using Spectral Ultrasound ImagingNoninvasive. PLoS ONE. 2014; 9:e85749. [PubMed: 24465680]
24. Hall TJ, Zhu Y, Spalding CS. In vivo real-time freehand palpation imaging. Ultrasound Med. Biol. 2003; 29:427–435. [PubMed: 12706194]
25. Herford AS, Boyne PJ, Williams RP. Clinical applications of rhBMP-2 in maxillofacial surgery. J. Calif. Dent. Assoc. 2007; 35:335–341. [PubMed: 17822159]
26. Herford AS, Lu M, Akin L, Cicciù M. Evaluation of a porcine matrix with and without platelet-derived growth factor for bone graft coverage in pigs. Int. J. Oral Maxillofac. Implants. 2012; 27:1351–1358. [PubMed: 23189284]
27. Hibino N, Duncan DR, Nalbandian A, Yi T, Qyang Y, Shinoka T, Breuer CK. Evaluation of the use of an induced puripotent stem cell sheet for the construction of tissue-engineered vascular grafts. J. Thorac. Cardiovasc. Surg. 2012; 143:696–703. [PubMed: 22244569]
28. Kang K-T, Allen P, Bischoff J. Bioengineered human vascular networks transplanted into secondary mice reconnect with the host vasculature and re-establish perfusion. Blood. 2011; 118:6718–6721. [PubMed: 22039257]
29. Kawamura M, Miyagawa S, Miki K, Saito A, Fukushima S, Higuchi T, Kawamura T, Kuratani T, Daimon T, Shimizu T, Okano T, Sawa Y. Feasibility, Safety, and Therapeutic Efficacy of Human Induced Pluripotent Stem Cell-Derived Cardiomyocyte Sheets in a Porcine Ischemic Cardiomyopathy Model. Circulation. 2012; 126:S29–S37. [PubMed: 22965990]
30. Kim K, Jeong CG, Hollister SJ. Non-invasive monitoring of tissue scaffold degradation using ultrasound elasticity imaging. Acta Biomater. 2008; 4:783–790. [PubMed: 18348913]
31. Kim K, Johnson LA, Jia C, Joyce JC, Rangwalla S, Higgins PDR, Rubin JM. Noninvasive Ultrasound Elasticity Imaging (UEI) of Crohn's Disease: Animal Model. Ultrasound Med. Biol. 2008; 34:902–912. [PubMed: 18294759]
32. Kim S, Chen Y-S, Luke GP, Emelianov SY. In vivo three-dimensional spectroscopic photoacoustic imaging for monitoring nanoparticle delivery. Biomed. Opt. Express. 2011; 2:2540. [PubMed: 21991546]
33. Konofagou E, Ophir J. A new elastographic method for estimation and imaging of lateral displacements, lateral strains, corrected axial strains and poisson's ratios in tissues. Ultrasound Med. Biol. 1998; 24:1183–1199. [PubMed: 9833588]
34. Kreitz S, Dohmen G, Hasken S, Schmitz-Rode T, Mela P, Jockenhoevel S. Nondestructive Method to Evaluate the Collagen Content of Fibrin-Based Tissue Engineered Structures Via Ultrasound. Tissue Eng. Part C Methods. 2011; 17:1021–1026. [PubMed: 21663456]
35. Kumar VA, Caves JM, Haller CA, Dai E, Li L, Grainger S, Chaikof EL. Acellular Vascular Grafts Generated from Collagen and Elastin Analogues. Acta Biomater. 2013; 9:8067–8074. [PubMed: 23743129]
36. Lee IS, Bourantas CV, Muramatsu T, Gogas BD, Heo JH, Diletti R, Farooq V, Zhang Y, Onuma Y, Serruys PW, Garcia-Garcia HM. Assessment of plaque evolution in coronary bifurcations located beyond everolimus eluting scaffolds: serial intravascular ultrasound virtual histology study. Cardiovasc. Ultrasound. 2013; 11:25. [PubMed: 23870248]

37. Lee WK, Ichi T, Ooya T, Yamamoto T, Katoh M, Yui N. Novel poly(ethylene glycol) scaffolds crosslinked by hydrolyzable polyrotaxane for cartilage tissue engineering. JBiomed Mater Res. 2002; 67 A:1087–1092.
38. Lerner, RM.; Parker, KJ.; Holen, J.; Gramiak, R.; Waag, RC. Sono-Elasticity: Medical Elasticity Images Derived from Ultrasound Signals in Mechanically Vibrated Targets. In: Kessler, LW., editor. Acoustical Imaging. Springer US: 1988. p. 317-327.at <http://link.springer.com/chapter/10.1007/978-1-4613-0725-9_31>
39. Lizzi FL, Astor M, Liu T, Deng C, Coleman DJ, Silverman RH. Ultrasonic spectrum analysis for tissue assays and therapy evaluation. Int. J. Imaging Syst. Technol. 1997; 8:3–10.
40. Lubinski MA, Emelianov SY, O'Donnell M. Speckle tracking methods for ultrasonic elasticity imaging using short-time correlation. IEEE Trans. Ultrason. Ferroelectr. Freq. Control. 1999; 46:82–96. [PubMed: 18238401]
41. Luke GP, Yeager D, Emelianov SY. Biomedical Applications of Photoacoustic Imaging with Exogenous Contrast Agents. Ann. Biomed. Eng. 2011; 40:422–437. [PubMed: 22048668]
42. Lyshchik A, Higashi T, Asato R, Tanaka S, Ito J, Hiraoka M, Insana MF, Brill AB, Saga T, Togashi K. Cervical Lymph Node Metastases: Diagnosis at Sonoelastography—Initial Experience. Radiology. 2007; 243:258–267. [PubMed: 17293571]
43. Martinez-Diaz S, Garcia-Giralt N, Lebourg M, Gómez-Tejedor J-A, Vila G, Caceres E, Benito P, Pradas MM, Nogues X, Ribelles JLG, Monllau JC. In Vivo Evaluation of 3-Dimensional Polycaprolactone Scaffolds for Cartilage Repair in Rabbits. Am. J. Sports Med. 2010; 38:509–519. [PubMed: 20093424]
44. Matsumura G, Nitta N, Matsuda S, Sakamoto Y, Isayama N, Yamazaki K, Ikada Y. Long-Term Results of Cell-Free Biodegradable Scaffolds for In Situ Tissue-Engineering Vasculature: In a Canine Inferior Vena Cava Model. PLoS ONE. 2012; 7
45. Maurice RL, Fromageau J, Brusseau É, Finet G, Rioufol G, Cloutier G. On the Potential of the Lagrangian Estimator for Endovascular Ultrasound Elastography: In Vivo Human Coronary Artery Study. Ultrasound Med. Biol. 2007; 33:1199–1205. [PubMed: 17466446]
46. McAleavey S, Menon M, Elegbe E. Shear Modulus Imaging with Spatially Modulated Ultrasound Radiation Force. Ultrason. Imaging. 2009; 31:217–234. [PubMed: 20458875]
47. McAllister TN, Maruszewski M, Garrido SA, Wystrychowski W, Dusserre N, Marini A, Zagalski K, Fiorillo A, Avila H, Manglano X, Antonelli J, Kocher A, Zembala M, Cierpka L, de la Fuente LM, L'Heureux N. Effectiveness of haemodialysis access with an autologous tissue-engineered vascular graft: a multicentre cohort study. The Lancet. 2009; 373:1440–1446.
48. Mercado KP, Helguera M, Hocking DC, Dalecki D. Estimating cell concentration in three-dimensional engineered tissues using high frequency quantitative ultrasound. Ann. Biomed. Eng. 2014; 42:1292–1304. [PubMed: 24627179]
49. Nair A, Kuban BD, Tuzcu EM, Schoenhagen P, Nissen SE, Vince DG. Coronary Plaque Classification With Intravascular Ultrasound Radiofrequency Data Analysis. Circulation. 2002; 106:2200–2206. [PubMed: 12390948]
50. Nam SY, Ricles LM, Suggs LJ, Emelianov SY. In vivo ultrasound and photoacoustic monitoring of mesenchymal stem cells labeled with gold nanotracers. PloS One. 2012; 7:e37267. [PubMed: 22615959]
51. Nam SY, Ricles LM, Suggs LJ, Emelianov SY. Nonlinear photoacoustic signal increase from endocytosis of gold nanoparticles. Opt. Lett. 2012; 37:4708–4710. [PubMed: 23164887]
52. Nam SY, Ricles LM, Suggs LJ, Emelianov SY. Imaging strategies for tissue engineering applications. Tissue Eng. Part B Rev. 2015; 21:88–102. [PubMed: 25012069]
53. Nasu K, Tsuchikane E, Katoh O, Vince DG, Virmani R, Surmely J-F, Murata A, Takeda Y, Ito T, Ehara M, Matsubara T, Terashima M, Suzuki T. Accuracy of In Vivo Coronary Plaque Morphology Assessment: A Validation Study of In Vivo Virtual Histology Compared With In Vitro Histopathology. J. Am. Coll. Cardiol. 2006; 47:2405–2412. [PubMed: 16781367]
54. Neumayer L, Giobbie-Hurder A, Jonasson O, Fitzgibbons R, Dunlop D, Gibbs J, Reda D, Henderson W. Open Mesh versus Laparoscopic Mesh Repair of Inguinal Hernia. N. Engl. J. Med. 2004; 350:1819–1827. [PubMed: 15107485]

55. Nguyen, MM.; Ding, X.; Yu, J.; Park, D.; Yu, F.; Kim, K. Tri-modality ultrasound imaging system: Design and phantom experiment results. 2014. doi:10.1109/ULTSYM.2014.0080
56. Nightingale K, McAleavey S, Trahey G. Shear-wave generation using acoustic radiation force: in vivo and ex vivo results. Ultrasound Med. Biol. 2003; 29:1715–1723. [PubMed: 14698339]
57. Nightingale K, Soo MS, Nightingale R, Trahey G. Acoustic radiation force impulse imaging: in vivo demonstration of clinical feasibility. Ultrasound Med. Biol. 2002; 28:227–235. [PubMed: 11937286]
58. Ntziachristos V. Going deeper than microscopy: the optical imaging frontier in biology. Nat. Methods. 2010; 7:603–614. [PubMed: 20676081]
59. O'Brien FJ. Biomaterials & scaffolds for tissue engineering. Mater. Today. 2011; 14:88–95.
60. O'Donnell M, Skovoroda AR, Shapo BM, Emelianov SY. Internal displacement and strain imaging using ultrasonic speckle tracking. IEEE Trans. Ultrason. Ferroelectr. Freq. Control. 1994; 41:314–325.
61. Ophir J, Céspedes I, Ponnekanti H, Yazdi Y, Li X. Elastography: A Quantitative Method for Imaging the Elasticity of Biological Tissues. Ultrason. Imaging. 1991; 13:111–134. [PubMed: 1858217]
62. Pan D, Pramanik M, Senpan A, Allen JS, Zhang H, Wickline SA, Wang LV, Lanza GM. Molecular photoacoustic imaging of angiogenesis with integrin-targeted gold nanobeacons. FASEB J. 2011; 25:875–882. [PubMed: 21097518]
63. Park DW, Ye S-H, Jiang HB, Dutta D, Nonaka K, Wagner WR, Kim K. In vivo monitoring of structural and mechanical changes of tissue scaffolds by multi-modality imaging. Biomaterials. 2014; 35:7851–7859. [PubMed: 24951048]
64. Perk G, Tunick PA, Kronzon I. Non-Doppler Two-dimensional Strain Imaging by Echocardiography–From Technical Considerations to Clinical Applications. J. Am. Soc. Echocardiogr. 2007; 20:234–243. [PubMed: 17336748]
65. Quint C, Arief M, Muto A, Dardik A, Niklason LE. Allogeneic human tissue-engineered blood vessel. J. Vasc. Surg. 2012; 55:790–798. [PubMed: 22056286]
66. Ribbers H, Lopata RGP, Holewijn S, Pasterkamp G, Blankensteijn JD, de Korte CL. Noninvasive Two-Dimensional Strain Imaging of Arteries: Validation in Phantoms and Preliminary Experience in Carotid Arteries In Vivo. Ultrasound Med. Biol. 2007; 33:530–540. [PubMed: 17280769]
67. Rice MA, Waters KR, Anseth KS. Ultrasound monitoring of cartilaginous matrix evolution in degradable PEG hydrogels. Acta Biomater. 2009; 5:152–161. [PubMed: 18793879]
68. Ricles LM, Nam SY, Sokolov K, Emelianov SY, Suggs LJ. Function of mesenchymal stem cells following loading of gold nanotracers. Int. J. Nanomedicine. 2011; 6:407–416. [PubMed: 21499430]
69. Rouze NC, Wang MH, Palmeri ML, Nightingale KR. Robust Estimation of Time-of-Flight Shear Wave Speed Using a Radon Sum Transformation. IEEE Trans. Ultrason. Ferroelectr. Freq. Control. 2010; 57:2662–2670. [PubMed: 21156362]
70. Rubin JM, Xie H, Kim K, Weitzel WF, Emelianov SY, Aglyamov SR, Wakefield TW, Urquhart AG, O'Donnell M. Sonographic elasticity imaging of acute and chronic deep venous thrombosis in humans. J. Ultrasound Med. Off. J. Am. Inst. Ultrasound Med. 2006; 25:1179–1186.
71. Sarvazyan AP, Rudenko OV, Swanson SD, Fowlkes JB, Emelianov SY. Shear wave elasticity imaging: a new ultrasonic technology of medical diagnostics. Ultrasound Med. Biol. 1998; 24:1419–1435. [PubMed: 10385964]
72. Skovoroda AR, Emelianov SY, Lubinski MA, Sarvazyan AP, O'Donnell M. Theoretical analysis and verification of ultrasound displacement and strain imaging. IEEE Trans. Ultrason. Ferroelectr. Freq. Control. 1994; 41:302–313.
73. Sun Y, Responte D, Xie H, Liu J, Fatakdawala H, Hu J, Athanasiou KA, Marcu L. Nondestructive Evaluation of Tissue Engineered Articular Cartilage Using Time-Resolved Fluorescence Spectroscopy and Ultrasound Backscatter Microscopy. Tissue Eng. Part C Methods. 2011; 18:215–226. [PubMed: 22010819]
74. Talukdar Y, Avti P, Sun J, Sitharaman B. Multimodal ultrasound-photoacoustic imaging of tissue engineering scaffolds and blood oxygen saturation in and around the scaffolds. Tissue Eng. Part C Methods. 2014; 20:440–449. [PubMed: 24107069]

75. Tanaka Y, Saijo Y, Fujihara Y, Yamaoka H, Nishizawa S, Nagata S, Ogasawara T, Asawa Y, Takato T, Hoshi K. Evaluation of the implant type tissue-engineered cartilage by scanning acoustic microscopy. J. Biosci. Bioeng. 2012; 113:252–257. [PubMed: 22138383]
76. Tayalia P, Mooney DJ. Controlled Growth Factor Delivery for Tissue Engineering. Adv. Mater. 2009; 21:3269–3285. [PubMed: 20882497]
77. Tillman BW, Yazdani SK, Neff LP, Corriere MA, Christ GJ, Soker S, Atala A, Geary RL, Yoo JJ. Bioengineered vascular access maintains structural integrity in response to arteriovenous flow and repeated needle puncture. J. Vasc. Surg. 2012; 56:783–793. [PubMed: 22917043]
78. Tsuji W, Inamoto T, Ito R, Morimoto N, Tabata Y, Toi M. Simple and longstanding adipose tissue engineering in rabbits. J. Artif. Organs. 2012; 16:110–114. [PubMed: 23114565]
79. VandeVord PJ, Matthew HWT, DeSilva SP, Mayton L, Wu B, Wooley PH. Evaluation of the biocompatibility of a chitosan scaffold in mice. J. Biomed. Mater. Res. 2002; 59:585–590. [PubMed: 11774317]
80. Wang LV, Hu S. Photoacoustic Tomography: In Vivo Imaging from Organelles to Organs. Science. 2012; 335:1458–1462. [PubMed: 22442475]
81. Weber M, Heta E, Moreira R, Gesche VN, Schermer T, Frese J, Jockenhoevel S, Mela P. Tissue-engineered fibrin-based heart valve with a tubular leaflet design. Tissue Eng. Part C Methods. 2014; 20:265–275. [PubMed: 23829551]
82. Wells PNT. Ultrasound imaging. Phys. Med. Biol. 2006; 51:R83. [PubMed: 16790922]
83. Weyhe D, Belyaev O, Müller C, Meurer K, Bauer K-H, Papapostolou G, Uhl W. Improving Outcomes in Hernia Repair by the Use of Light Meshes—A Comparison of Different Implant Constructions Based on a Critical Appraisal of the Literature. World J. Surg. 2006; 31:234–244. [PubMed: 17180568]
84. Winterroth F, Hollman KW, Kuo S, Ganguly A, Feinberg SE, Fowlkes JB, Hollister SJ. Characterizing morphology and nonlinear elastic properties of normal and thermally stressed engineered oral mucosal tissues using scanning acoustic microscopy. Tissue Eng. Part C Methods. 2013; 19:345–351. [PubMed: 23072525]
85. Winterroth F, Hollman KW, Kuo S, Izumi K, Feinberg SE, Hollister SJ, Fowlkes JB. Comparison of scanning acoustic microscopy and histology images in characterizing surface irregularities among engineered human oral mucosal tissues. Ultrasound Med. Biol. 2011; 37:1734–1742. [PubMed: 21871704]
86. Wu W, Allen RA, Wang Y. Fast-degrading elastomer enables rapid remodeling of a cell-free synthetic graft into a neoartery. Nat. Med. 2012; 18:1148–1153. [PubMed: 22729285]
87. Wystrychowski W, McAllister TN, Zagalski K, Dusserre N, Cierpka L, L'Heureux N. First human use of an allogeneic tissue-engineered vascular graft for hemodialysis access. J. Vasc. Surg. 2014; 60:1353–1357. [PubMed: 24103406]
88. Yoshikawa M, Yabuuchi T, Tsuji N, Shimomura Y, Hayashi H, Ohgushi H. In Vivo Osteogenesis in Porous Hydroxyapatite Scaffold Processed in Hyaluronic Acid Solution. Key Eng. Mater. 2008; 361-363:1185–1188.
89. Yu J, Takanari K, Hong Y, Lee K-W, Amoroso NJ, Wang Y, Wagner WR, Kim K. Noninvasive characterization of polyurethane-based tissue constructs in a rat abdominal repair model using high frequency ultrasound elasticity imaging. Biomaterials. 2013; 34:2701–2709. [PubMed: 23347836]
90. Zhang Y, Cai X, Choi S-W, Kim C, Wang LV, Xia Y. Chronic label-free volumetric photoacoustic microscopy of melanoma cells in three-dimensional porous scaffolds. Biomaterials. 2010; 31:8651–8658. [PubMed: 20727581]
91. Zhang Y, Cai X, Wang Y, Zhang C, Li L, Choi S-W, Wang LV, Xia Y. Noninvasive Photoacoustic Microscopy of Living Cells in Two and Three Dimensions through Enhancement by a Metabolite Dye. Angew. Chem. Int. Ed. 2011; 50:7359–7363.
92. Zhang YS, Cai X, Yao J, Xing W, Wang LV, Xia Y. Non-invasive and in situ characterization of the degradation of biomaterial scaffolds by volumetric photoacoustic microscopy. Angew. Chem. Int. Ed Engl. 2014; 53:184–188. [PubMed: 24130155]

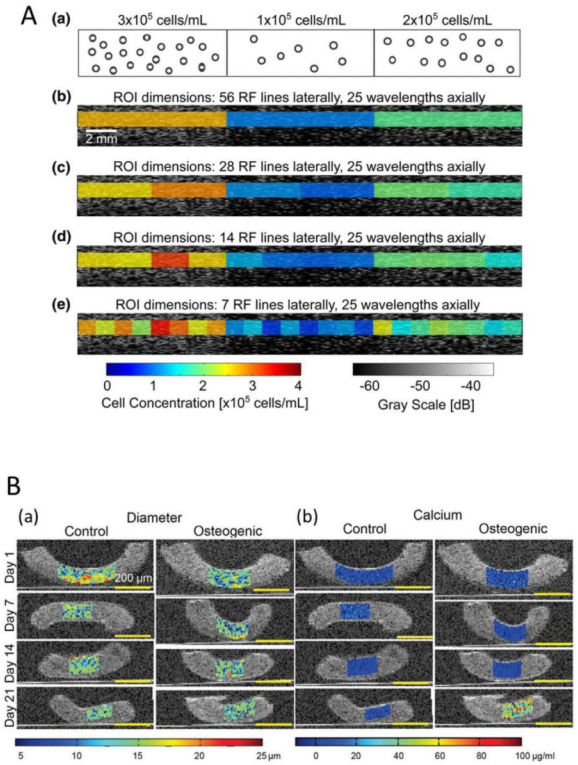

Figure 1.

Panel A: Imaging agarose gels fabricated with three distinct regions of homogeneous distribution of mouse embryonic fibroblasts at different concentrations of 3×10^5, 1×10^5, and 2×10^5 cells/mL, (a). Representative B-mode (gray scale) image of an agarose gel, and overlaid parametric images of cell concentrations in regions of interest (ROIs) that have (b) 56, (c) 28, (d) 14, and (e) 7 radiofrequency (RF) data lines. Data were acquired using the 38-MHz transducer. The linear regression equation of the integrated backscattering coefficient (IBC) as a function of cell concentration was used to convert IBC values to corresponding cell concentration estimates. Each ROI had an axial dimension of 25 wavelengths. Adapted from Fig. 8.[48] Panel B: Overlaid B-mode (grayscale) and color maps of high resolution spectral ultrasound imaging (SUSI) parameters. The changes in (a) cell diameter, and (b) mass of calcium deposition of MC3T3 cells embedded in collagen constructs in control and osteogenic media were monitored in vitro over the time period of 21 days. Adapted from Fig. 8.[23]

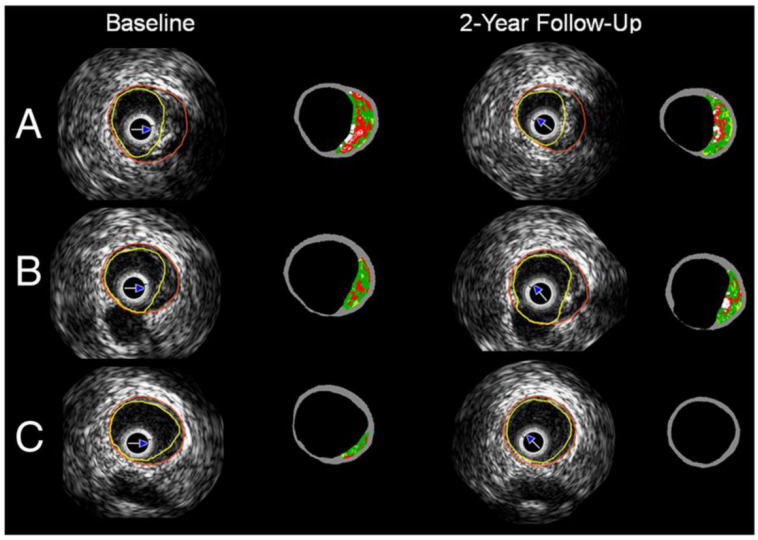

Figure 2.

A typical IVUS-virtual histology (VH) on the bifurcation segment at baseline and at 2 years follow-up of human subjects with obstructive coronary artery diseases who underwent percutaneous coronary intervention with the everolimus-eluting bioresorbable vascular scaffold. A The proximal rim of the ostium of the side branch, B the in-bifurcation segment and C the distal rim of the ostium of the side branch are shown. The white color corresponds to the calcified tissue, the red to the necrotic core, the light green to the fibro fatty and the green to fibrotic tissue. Adapted from Fig. 2.[36]

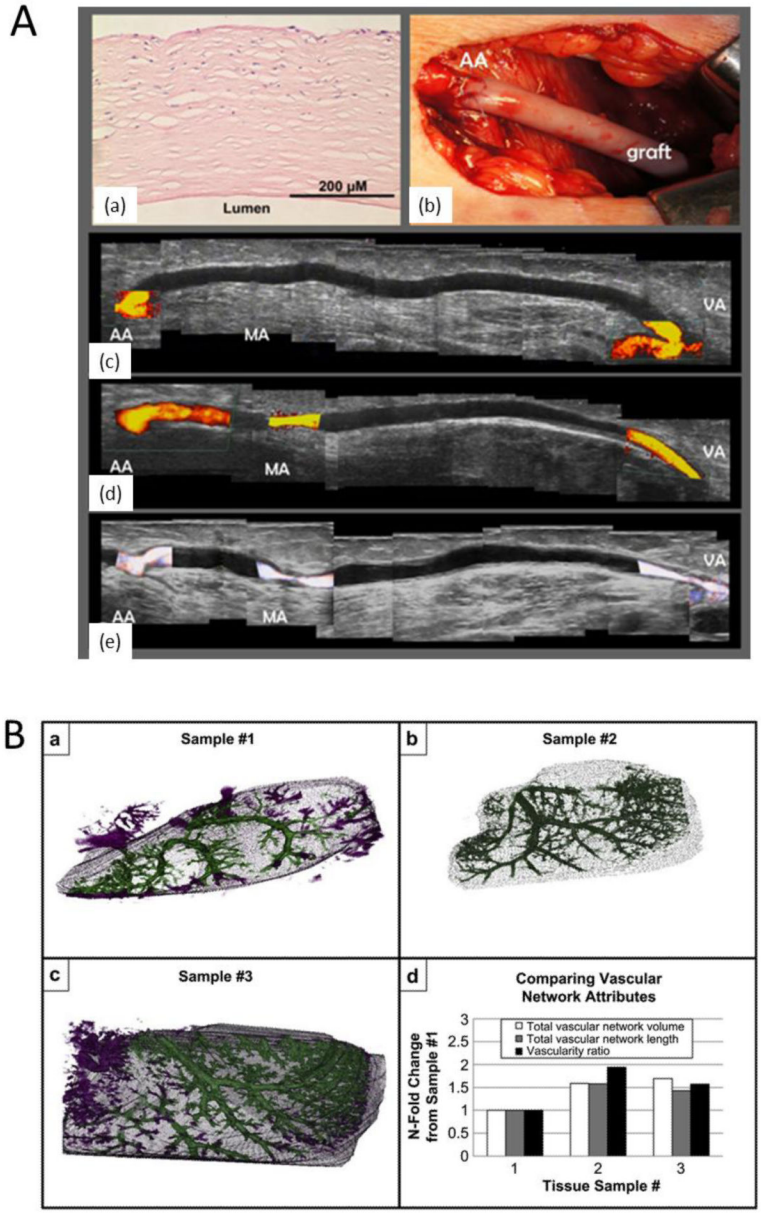

Figure 3.

Panel A: Ultrasound imaging used clinically with an acellular hemodialysis access graft implanted as a shunt in an 80-year-old female patient with glomerulonephritis and coronary artery disease. She had been receiving hemodialysis for 4.5 years, with previous failures of an ambilateral brachial-cephalic access and of tunneled hemodialysis catheters in multiple locations, recurrent catheter infections and thromboses, hospitalizations for pneumonia, and lower limb deep venous thrombosis. (a) Preimplantation hematoxylin and eosin staining of the devitalized graft. (b) Macroscopic view shows the implanted graft. Doppler ultrasound results at (c) 1 month, (d) 6 months, and (e) 11 months (composites from scan of entire length of graft) demonstrating no evidence of aneurysm or wall degradation. At 11 months (e), restenosis was noted near the medial anastomosis (MA), 6 months after percutaneous

transluminal angioplasty. Flow shown in color was 1.3, 0.7, and 0.4 L/min at 1, 6, and 11 months, respectively. AA, Arterial anastomosis; VA, venous anastomosis; MA, medial anastomosis. Adapted from Fig.1.[87] Panel B: Vessel networks are visualized from a-c) 3D renderings of in vitro acoustic angiography obtained by vessel segmentation, after injecting microbubbles in an extracellular matrix scaffold prepared by decelluarizing a rat liver. Three samples were prepared. Color is defined as either inside (green) or outside (purple) of the manually defined construct border. d) Quantitative assessments of vascular network volume, length, and vascularity ratio. Data are normalized to sample #1 for comparison purpose. Adapted from Fig. 4.[21]

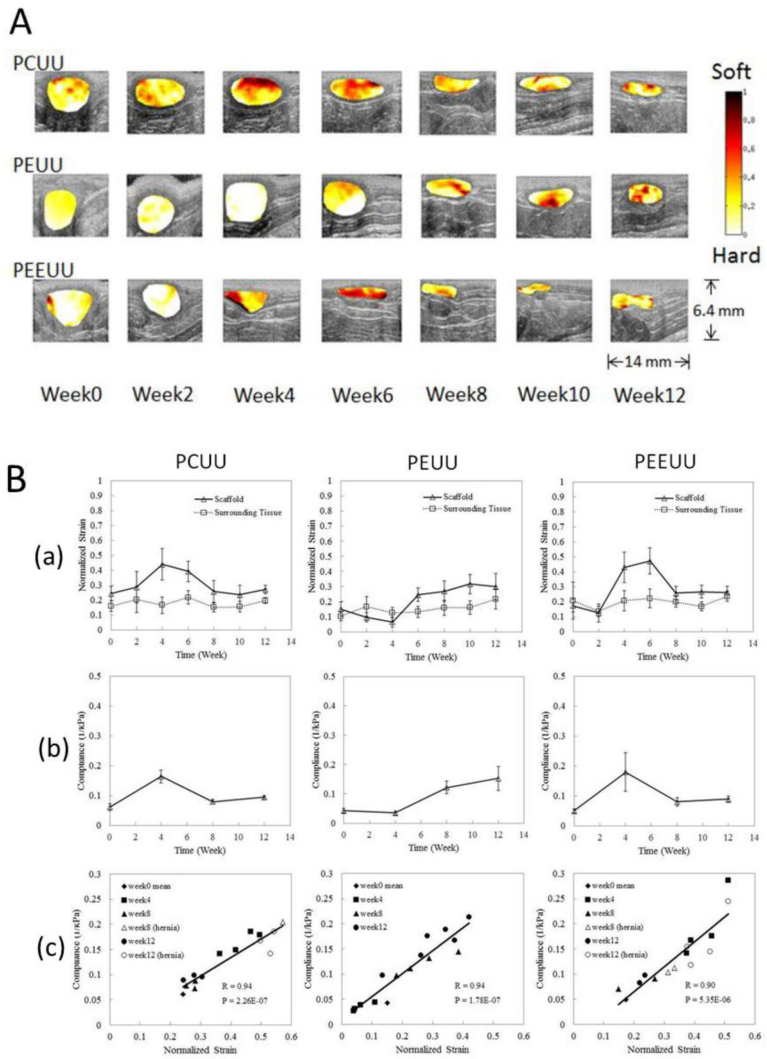

Fig. 4.

Panel A: Normalized strain map (in color) laid over B-mode images (morphology) of degradable elastomeric scaffolds implanted to replace the rat abdominal wall. Average strain and compliance over time. Panel B: (a) Normalized strain obtained from UEI for scaffold averaged over 8 samples (except when scaffold develops hernia) and surrounding tissue over time. (b) Mean compliance (1/elastic modulus) from compression tests. (c) Scatter plots of the compliance and normalized strain values based on the same samples at corresponding time points. R denotes correlation coefficient and P indicates the p-value for the correlation between compliance and normalized strain. Samples with hernia are represented by open symbols. Adapted from Fig. 3.[89]

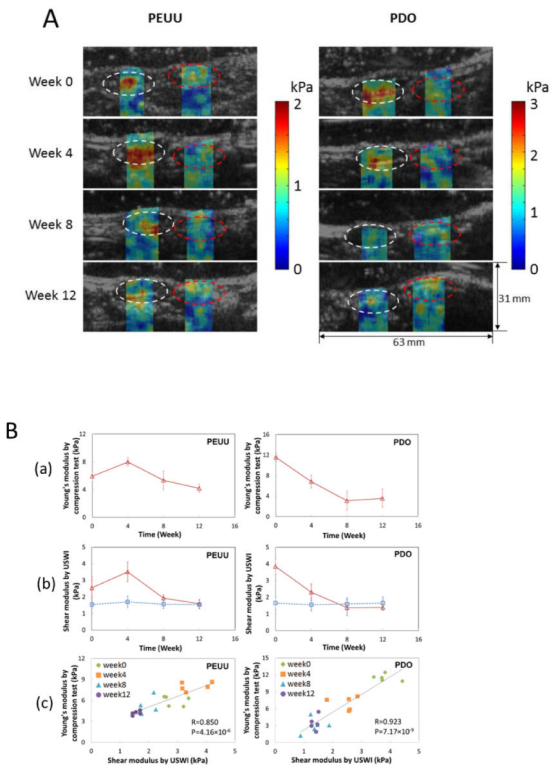

Fig. 5.

Panel A: Shear modulus maps reconstructed using USWEI for two types of polymeric scaffolds (PEUU and PDO) that were implanted in the rat abdominal wall and overlaid B-mode images over implantation period. White and red dashed circles denote the engineered tissue construct and surrounding native tissue, respectively. Panel B: Elastic modulus obtained by USWEI compared with direct compression measurements. Panel B: (a) Young's modulus obtained by compression tests using a commercial testing machine. (b) Average shear modulus of the constructs (red open triangle) and native tissue (blue open square) obtained by USWEI over implantation period. (c) Scatter plots presents the relation between the Young's modulus and shear modulus from the same samples for corresponding implantation time periods. R denotes the correlation coefficient and P represents the p-value for the correlation between the Young's modulus (a) and shear modulus (b). Adapted from Figures 3 & 4.[63]

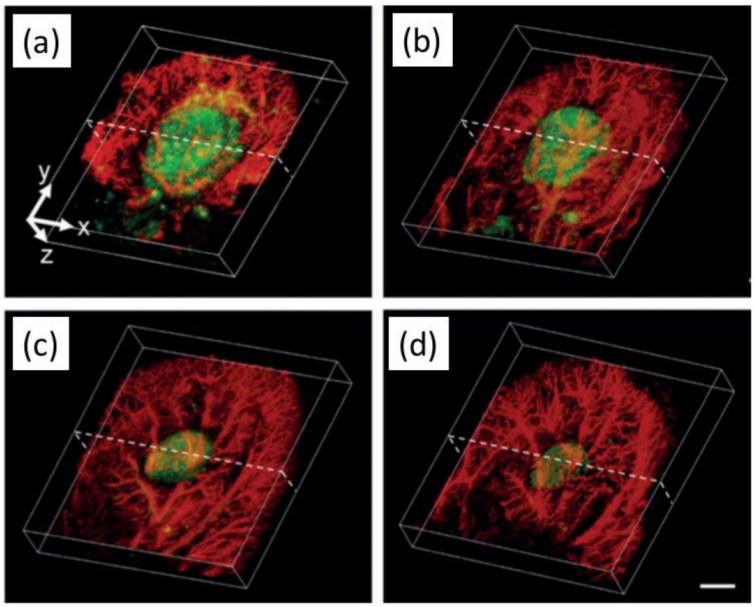

Figure 6.

Both scaffold (green in the middle) degradation and vascular remodeling (red in the periphery) viewed in co-registered 3D reconstructed acoustic resolution photoacoustic microscopy (AR-PAM) images obtained at two different wavelengths (578 nm, 638nm). (a-d) Images were taken from a poly(lactide-co-glycolide) inverse opal scaffold implanted in the ear of a nude mouse for 0, 1, 3, and 6 weeks, respectively. Scale bars: 2 mm. Adapted from Fig. 4.[92]

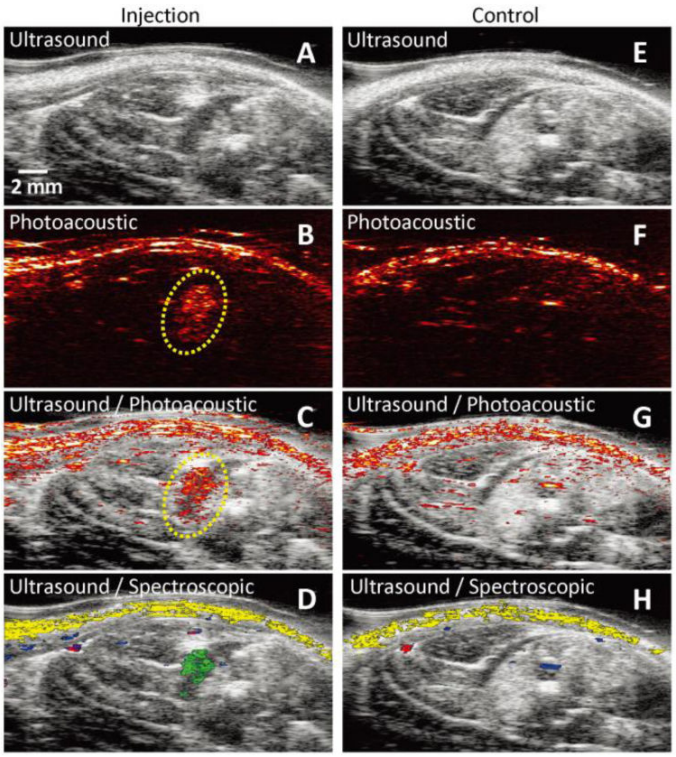

Figure 7.

In vivo tracking of gold nanotracers (Au NT) labeled mesenchymal stem cells (MSCs) intramuscularly injected in the lower limb of the Lewis rat, using combined ultrasound and photoacoustic (US/PA) imaging. The ultrasound image shows the structural information of the lower limb, but the location of MSCs cannot be identified. However, the photoacoustic and US/PA images clearly show the location of the nanotracer signal from MSCs in the gel outlined in yellow (B). (A–D) In vivo ultrasound, photoacoustic, US/PA, and US/spectroscopic images of the lateral gastrocnemius (LGAS) in which PEGylated fibrin gel containing Au NT loaded MSCs (1×10^5 cells/mL) was injected. The gel location is outlined with yellow dotted circle. Injection depth was about 5 mm under the skin. (E–H) Control at the region of the LGAS of the other hind limb without any injection. Spectral (650–920 nm) analysis of photoacoustic signal was able to differentiate skin (shown in yellow), oxygenated (red) and deoxygenated (blue) blood, and Au NT loaded MSCs (green). The images measure 23 mm laterally and 12.5 mm axially. Adapted from Fig. 6. [50]

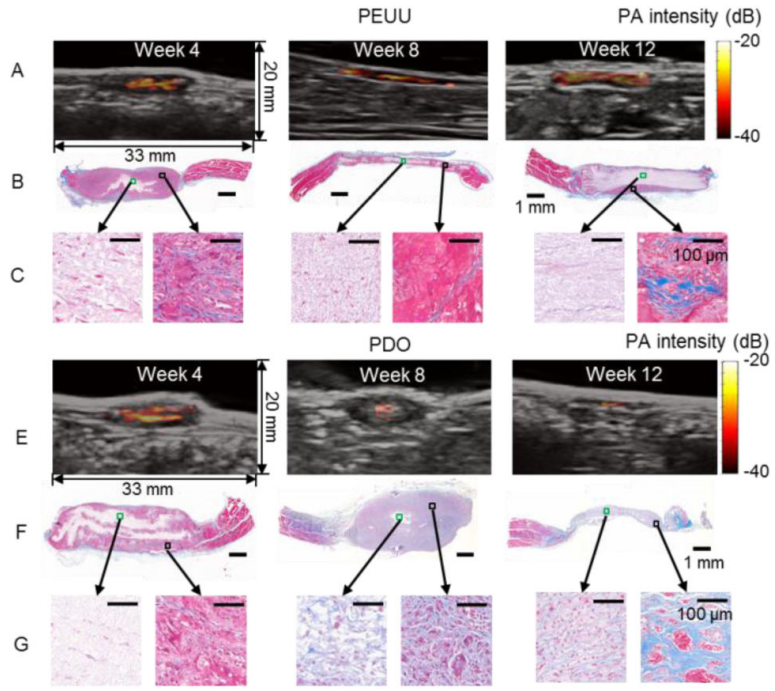

Figure 8.

Photoacoustic images that identify scaffold remainders (bright red-yellow-white) overlaid on B-mode anatomical images that locate implant sites (hypoechoic areas in gray scale) for the PEUU (A) and PDO (E) constructs implanted in in the rat abdominal wall at 4, 8 and 12 weeks. Masson's trichrome staining of PEUU (B) and PDO (F) constructs. Representative areas in the central (green box) and peripheral (black box) regions of PEUU (C) and PDO (G) constructs are magnified. Adapted from Fig. 4.[63]

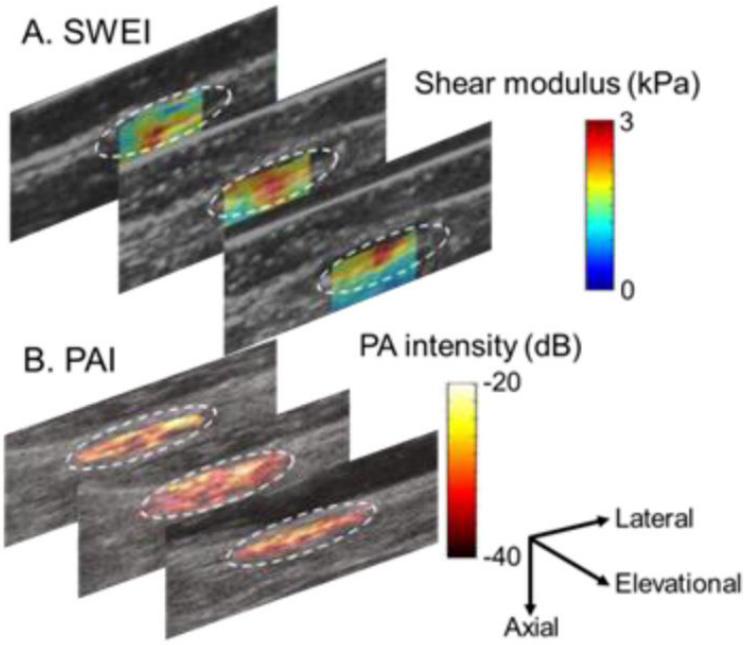

Figure 9.

Co-registered ultrasound swear wave elasticity images that represent shear elastic modulus map (A) and photoacoustic images that identify scaffold remainders (B) overlaid on B-mode images for anatomy of a PDO scaffold implanted for 4 weeks. 2D imaging planes are separated by ~2 mm. White circles trace the implant sites.

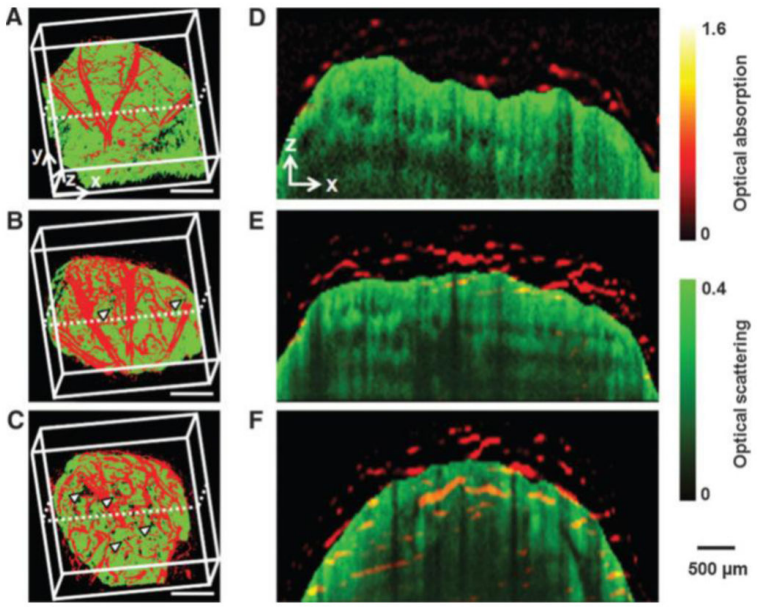

Figure 10.

Optical resolution photoacoustic microscopy (OR-PAM) and optical coherence tomography (OCT) co-registered images showing the development of neovasculature (red) and scaffold/tissue construct (green) at 2 (A), 4(B), and 6(C) weeks after implantation of Poly(d, l-lactide-co-glycolide) (PLGA) inverse opal scaffold in the nude mouse ear. Arrowheads indicate the growth of neovasculature into the scaffold pores (scale bars: 500 mm). (D–F) Co-registered B-scan images at the planes indicated by dotted lines in (a–d), respectively, showing the blood vessel growth into the inner scaffold pores. Adapted from Fig. 3.[8]